

# Scaling atom array assembly with grey molasses

M. O. Brown,\* T. Thiele,\* C. Kiehl, T.-W. Hsu, and C. A. Regal<sup>†</sup>  
*JILA, National Institute of Standards and Technology and University of Colorado,  
 and Department of Physics, University of Colorado, Boulder, Colorado 80309, USA*

We show that with a purely blue-detuned cooling mechanism we can densely load single neutral atoms into large arrays of shallow optical tweezers. With this ability, more efficient assembly of larger ordered arrays will be possible - hence expanding the number of particles available for bottom-up quantum simulation and computation with atoms. Using  $\Lambda$ -enhanced grey molasses on the D<sub>1</sub> line of <sup>87</sup>Rb, we achieve loading into a single 0.63 mK trap with 89% probability, and we further extend this loading to 100 atoms at 80% probability. The loading behavior agrees with a model of consecutive light-assisted collisions in repulsive molecular states. With simple rearrangement that only moves rows and columns of a 2D array, we demonstrate one example of the power of enhanced loading in large arrays.

In quantum simulation and computing, the assembly of large arrays of individually-controllable particles is a frontier challenge. Ultracold gases of neutral atoms have long simulated quantum physics on a macroscopic scale, and quantum gas microscopes are now a window to microscopic dynamics [1, 2]. However, the desire for control of individual atoms, in particular for quantum computing, motivates pursuing a bottom-up engineering approach [3–6]. Implementations of a Maxwell’s demon based upon single atom imaging and rearranging have presented new opportunities in studies of multi-particle quantum dynamics [7–15], but compared to trapped ions, neutral atoms are still difficult to trap individually. In our work, we combine dense loading of large optical tweezer arrays using  $\Lambda$ -enhanced grey molasses (AGM) with atom imaging and rearrangement to form ordered atom arrays [16, 17]. With AGM we load single atoms with 89(1)% efficiency in traps shallower than required for standard sub-poissonian loading [18] and nearly an order of magnitude shallower than required for previous enhanced loading [19]. Our key insight was to use blue-detuned cooling to photoassociate atoms exclusively to repulsive molecular states. Our technique will scale up neutral-atom array assembly by expanding rearrangement algorithms and by enabling considerably larger ordered arrays.

To isolate single atoms in optical tweezers or lattices, it is standard practice to drive light-assisted collisions in the collisional blockade regime using red-detuned light [18, 20]. Here, atoms are photoassociated to attractive molecular states in which they accelerate towards each other and gain kinetic energy that predominantly expels both from the trap [Fig. 1(a)]. If the collisions occur quickly enough to dominate the dynamics, as is the case in microtraps, a single atom is left about half the time. In the pioneering work of Ref. [19], after adding a blue-detuned laser to drive atoms into repulsive molecular states, the energy gained in the collision was tuned to induce single atom loss [19, 21–23]. Loading efficiency was enhanced to 90%, but at the cost of requiring large trap depths ( $U/k_B \sim 3$  mK compared to 1 mK for red-

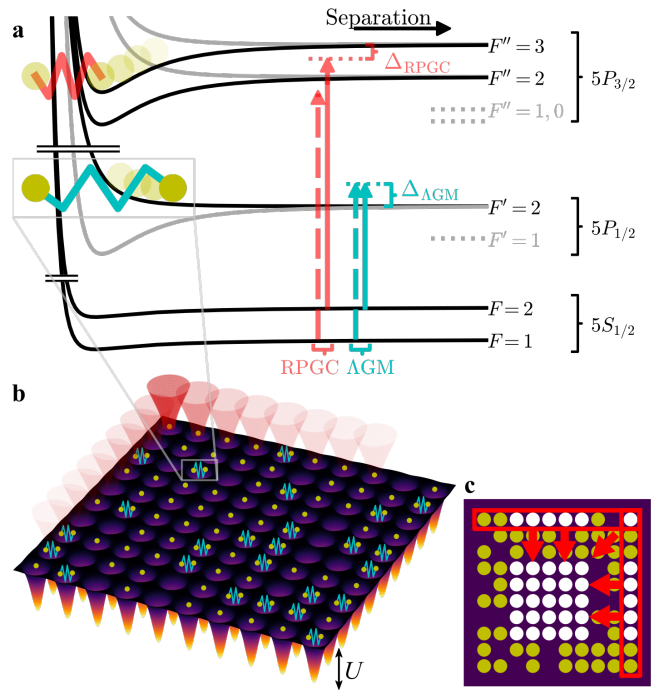


FIG. 1. Enhanced loading and rearrangement in large arrays. (a) Sketch of laser configuration, and molecular energies versus interatomic separation. Solid (dashed) arrows show cooling (repump) lasers with indicated detunings. (b) Atoms loaded into an array of 100 traps with depth  $U$  formed by optical tweezers undergo blue-detuned light-assisted collisions. (c) Schematic of parallel rearrangement to form defect-free array with target atoms (white) after removing a subset of loaded atoms (yellow).

detuned loading) making use of the technique difficult in large arrays.

A common theme in enhanced loading to-date is that the red-detuned lasers required for cooling still drive lossy collisions in conflict with desired blue-detuned collisions. Here we resolve this conflict by cooling and photoassociating with the same blue-detuned laser [Fig. 1(a)]. After the blue-detuned cooling modifies the atom number dis-

tribution, we apply red-detuned light, which both assures only single atoms remain and images the atoms. A single optical tweezer with a trap depth of  $U/k_B = 0.63$  mK is loaded with 89(1)% efficiency, and a  $10 \times 10$  array is loaded with 80.49(6)% efficiency [Fig. 1(b)]. Dense loading could also be used in optical lattices or in microtraps in 3D [14, 15]. We also demonstrate a proof-of-principle rearrangement technique that relies on the enhanced loading to create a  $6 \times 6$  defect-free array using a simplified sequence of parallel moves of entire rows and columns [Fig. 1(c)] [9].

For a blue-detuned cooling mechanism, we use  $\Lambda$ -enhanced grey molasses (AGM) [16, 17] for which the cooling laser is set blue-detuned of a type-2 ( $F' \leq F$ ) transition and in a  $\Lambda$  configuration with a coherent repump laser [Fig. 1(a)]. Because of its greater isolation from nearby hyperfine manifolds, we chose to operate the AGM detuned from the  $5P_{1/2}|F' = 2\rangle$  state [in contrast to, e.g.  $5P_{3/2}|F'' = 2\rangle$ ]. Note, we were motivated to use AGM mainly as a natural way to blue-detune both cooling and repump lasers, which is a somewhat different motivation than in recent quantum degenerate gas experiments with light atoms and molecules – namely that grey molasses works on open transitions, and  $\Lambda$ -enhancement results in lower temperatures [16, 17, 24–33].

We first present results from loading a single optical tweezer using AGM, and compare to standard loading using red-detuned polarization gradient cooling (RPGC) [Fig. 2(b,c)]. We capture  $^{87}\text{Rb}$  atoms in a magneto-optical trap (MOT), cool them into a spatially-overlapped optical tweezer with depth  $U$  with either AGM or RPGC, and then image the atoms with RPGC [Fig. 2(a)]. See Fig. 1(a) and the Appendix for laser configurations. The procedure is repeated to determine average loading efficiencies (see Appendix) [34]. Fig. 2(b,c) shows the loading probability  $P$  as a function of both detuning and trap depth for RPGC and AGM. With AGM we observe 89(1)% loading efficiency at  $(\Delta_{\text{AGM}}, U/k_B) = (45 \text{ MHz}, 0.55 \text{ mK})$ , and we can still load with  $\sim 80\%$  efficiency at trap depths of  $U/k_B \approx 0.27$  mK. These findings are remarkable as with the same optical power we can load tweezer arrays that are more densely filled *and* two to three times larger compared to RPGC loading. The maximum RPGC loading of 64(1)% for  $(\Delta_{\text{RPGC}}, U/k_B) \approx (-14 \text{ MHz}, 1.1 \text{ mK})$  is among the highest reported for RPGC [9, 10, 22, 23]. In the simplest picture of RPGC, one expects 50% loading, but, in agreement with other studies [23], additional processes result in  $\sim 35\%$  of the collisions causing only one atom to leave the trap.

A physically rich picture can be gained from studying the detuning dependence of AGM loading [Fig. 2(c)]. First, note that the trap light results in an AC Stark shift  $\delta_{\text{trap}} = 32.8 \frac{\text{MHz}}{\text{mK}} \frac{U}{k_B}$  of the atomic transition in the center of the trap [green lines in Fig. 2(c,d,f)]. The blue line in Fig. 2(c,d,f), which marks a shift of  $2U/h$  from the trap

shifted resonance, is a key energy scale for the physics of the enhanced loading. At shifts smaller than  $2U/h$ , the collision does not give a pair of zero-temperature atoms sitting at the bottom of the trap enough energy for either to escape, while at larger detunings both atoms will be expelled. A finite temperature, and hence an initial center of mass motion, will blur the transition, and indeed is necessary for inducing the desired single-atom loss. Although our data are roughly consistent with this picture, we look more closely by plotting the data of Fig. 2(c) against a dimensionless detuning  $h(\Delta_{\text{AGM}} - \delta_{\text{trap}})/U$ . We do this for all data traces  $U/k_B \geq 0.65$  mK [Fig. 2(d)], and observe a number of interesting features, one of which is that the maximum loading peaks below the  $2U/h$  shift (blue line).

To elucidate detailed trends, we have carried out a Monte-Carlo calculation of the collision dynamics. Most generally, we expect loading to be affected by both collisions and the AGM cooling performance, and both may be influenced by the non-trivial light shifts and polarization gradients in the tweezer traps. Modeling the interplay of these effects is beyond the scope of this letter, but we can understand the collisional process quantitatively if we assume the continuous AGM cooling can load at least a few atoms per trap, and re-thermalizes any atoms remaining after a collision. The simulation starts by preparing a Poisson-distributed number of atoms  $N_{\text{atom}}$  with a mean number  $\bar{N}_{\text{atom}} = 5$  and temperature  $T$ , where  $\bar{N}_{\text{atom}}$  was chosen  $> 2.5$  to avoid loading zero atoms initially. To simulate the finite experiment cooling time, we calculate a finite number of 5000 time steps each having two atoms collide once if they are closer than 100 nm. A collision might eject none, one, or both atoms out of the trap depending on the final energy of each atom, which is determined by their pre-collision energy and the collisional energy gain  $E = h[\Delta_{\text{AGM}} - \delta_{\text{atom}}]$ . This process continually reduces  $N_{\text{atom}}$  in each time step. At the end, the RPGC imaging is simulated by assuming that it entails a fast collisional process at the start of the image where red-detuned collisions reduce atom numbers in a manner consistent with our red loading – namely we reduce any remaining  $N_{\text{atom}} > 1$  by 2 with a chance of 65% and by 1 with a chance of 35% until  $N_{\text{atom}} \leq 1$ .

Fig. 2(d) shows the result of the Monte-Carlo simulation: During AGM-loading, the initial atom number (red dashed line) is reduced (cyan line). During RPGC imaging the  $\bar{N}_{\text{atom}}$  is further reduced [red line in Fig. 2(d)]. Fig. 2(e) shows how AGM and RPGC modify the Poisson distribution. We observe three physical regimes: For  $E \ll 2U$ , little atom loss occurs during the AGM, but the imaging step reduces the number of atoms to 0 or 1, yielding a RPGC-like 65% loading. In contrast, for  $E \gg 2U$ , two-body losses dominate resulting in  $\sim 50\%$  loading efficiency. At the transition  $E \approx 2U$ , both single atom and two-body losses occur with roughly equal probability, and the reason why the maximal loading probability

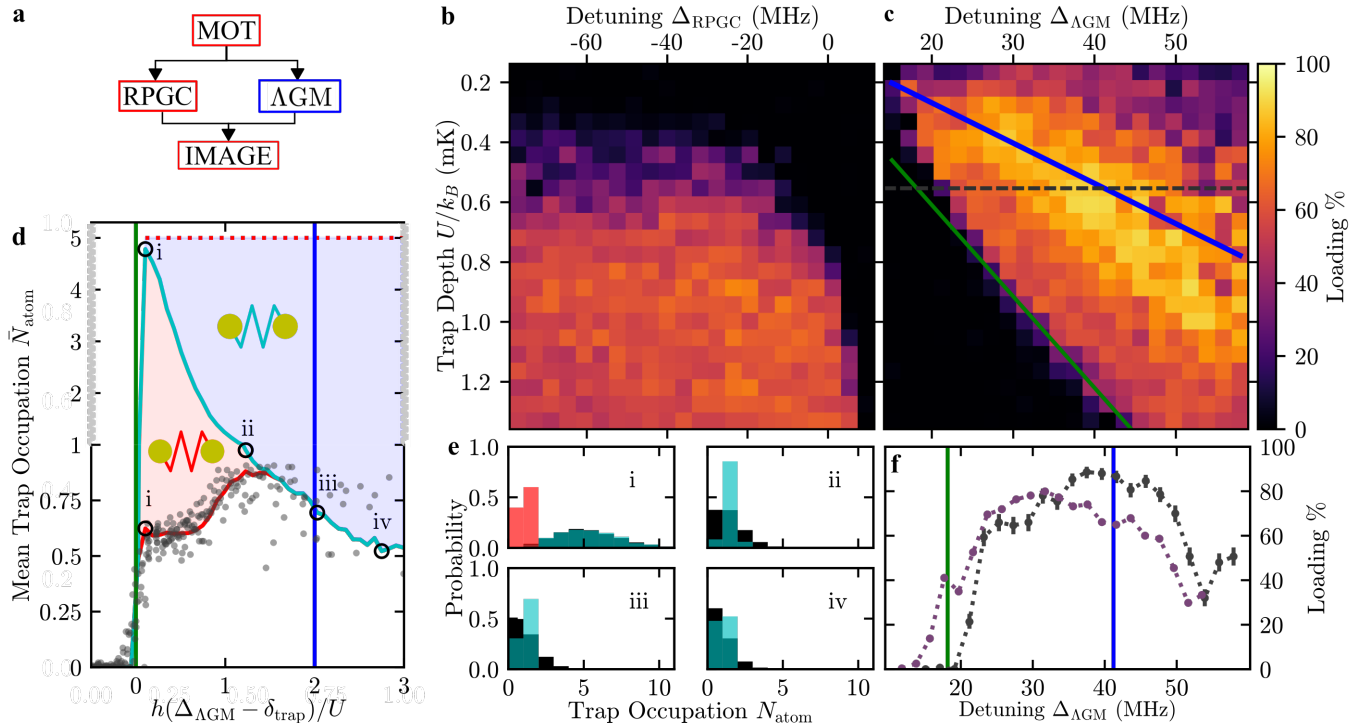


FIG. 2. AGM comparative loading studies. (a) Flow-diagram of experiments. (b,c) Average loading efficiency in a single optical tweezer from 150 experiment repetitions for RPGC (b) and AGM (c). (d) Monte-Carlo simulated mean trap occupation with bi-linear vertical scale (black and grey axes). In the AGM-step, the initial trap occupation (dashed, red line) is reduced (cyan line) by blue-detuned collisions (blue area). In the RPGC imaging step, red collisions (red area) further reduce the trap occupation (red line). The resultant is compared with data (grey points) from (c) averaged for  $U/k_B > 0.65$  mK (see text). (e) Histograms (cyan) of trap occupancy from the Monte-Carlo after the AGM-step for detunings indicated by the black circles in (d), compared to a Poisson-distribution (black) with the same mean trap occupation, and atom distribution after the RPGC-step (red in i). (f) Cut of loading data for a single tweezer (black) and a regular array of 100 tweezers (purple) at  $U/k_B \approx 0.55$  mK [black dashed line in (b)]. Error bars indicate statistical  $1\sigma$ -confidence interval (see Appendix). Throughout panels, green lines are AC-Stark-shifted  $|F = 2\rangle - |F'' = 3\rangle$  transition (for RPGC) and AC-Stark-shifted  $|F = 2\rangle - |F' = 2\rangle$  transition (for AGM), and blue lines are  $\delta_{\text{trap}} + 2U/h$ .

is found at  $E < 2U$  is because of the finite temperature and the fact that lower detunings favor one-body loss over two-body loss. Our model indicates no fundamental limitations to the loading efficiency and that by optimizing the trap size, atom temperature, and related parameters, it may be possible to reach higher loading fractions. Note that the simulation allows us to fit a mean atom temperature of  $T = 120(10)$   $\mu\text{K}$  to our measured data. This value is consistent with the free-space AGM temperature we measure of  $T \approx 50$   $\mu\text{K}$ , which is higher than typical values, likely due to non-ideal beam geometries (see Appendix).

We have also performed a loading study for an array of  $10 \times 10$  optical tweezers, of which we display the measurement at  $U/k_B = 0.55$  mK [purple in Fig. 2(f)]. Compared to the single-trap data at similar  $U$  (black), the data are shifted to smaller detunings, and we observe a maximum loading of  $80.49(6)\%$ . These effects could be due to a variety of consequences of the larger array: variations in trap shape and depth or overall degradations of

the optical spot sizes (see Appendix).

We now present an example of how dense loading opens up new opportunities in rearrangement algorithms for array assembly. After densely loading the array, we first obtain the location of each atom using a single image [left panel Fig. 3(a)]. Even with dense loading, the probability of loading a specific set of  $6 \times 6$  traps is exponentially small [dashed lines in Fig. 3(b)]. However, there are many potential sets of (sometimes disjoint)  $6 \times 6$  traps embedded in the  $10 \times 10$  array. We then search for such a configuration of completely loaded  $6 \times 6$  traps. If successful, we turn off the extra traps to remove the excess atoms, and then contract and shift the identified disjoint array in a *single* move (right panel) [9]. Currently, successful rearrangement to a square  $n = 36$  array only works in 0.1% of cases due to unexpected loss observed when turning off rows and columns, in which an atom is effectively lost with a 17%-chance. But, as illustrated in Fig. 3(b), observing this array with this parallel technique would have been impossible without enhanced

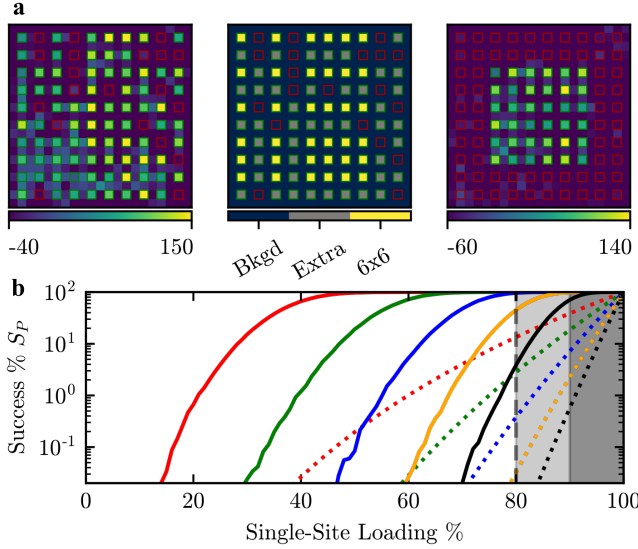


FIG. 3. Parallel rearrangement in 2D. (a) Single image of 80 atoms in an array of 100 traps with separation  $2 \mu\text{m}$  (left). Binarized loading (center) indicating empty traps (red squares), occupied traps (grey pixels), and loaded traps selected for parallel rearranging (yellow pixels) to a defect-free  $6 \times 6$  array. For the single-shot images, in each trap pixel (background pixel) the atom count threshold (average threshold of nearest neighbors) is subtracted for clarity. (b) Monte-Carlo-simulated probabilities of finding a filled disjoint array of atoms within  $10 \times 10$  traps as a function of loading efficiencies (solid lines), and corresponding loading probability of a specific array without rearrangement (dashed lines). Colors indicate target array sizes:  $3 \times 3$  (red),  $4 \times 4$  (green),  $5 \times 5$  (blue),  $6 \times 6$  (orange), and  $7 \times 7$  (black).

loading. In going from  $P = 60\%$  to  $P = 80\%$ , the percentage of experiment runs in which one could possibly extract a defect-free  $6 \times 6$  array goes from 0.02% to 37%. Notably, this entire procedure is completed using only a pair of acousto-optic modulators to control the optical tweezers.

The full potential of dense loading using grey molasses will likely come when combined with the most advanced atom-by-atom rearrangement algorithms in 2D or 3D [10, 14, 15]. Because AGM loading is efficient in shallow traps, more loadable traps can be created with the same amount of optical power. Additionally, 2D algorithms fill defects in a target array of size  $n$  with a sequence of  $m \propto (1-P)n^{1.4}$  single moves, which we verified with Monte-Carlo simulations [10]. In scaling up array sizes, the time and number of moves required becomes lengthy, lowering the probability of successful rearrangement ( $S_P$ ) as errors  $\epsilon$  due to finite move fidelities and background collisions suppress this success rate as  $e^{-m\epsilon}$  [10]. Increasing the loading probability from  $P = 60\%$  to  $P = 90\%$  would decrease  $m$  by a factor of 4, making larger array sizes more obtainable and exponentially improving the success probability  $S_P$ .

In conclusion, by gaining control over photoassociation to molecular states we have demonstrated enhanced loading of arrays of shallow optical tweezers. We have studied one particular blue-detuned cooling mechanism – AGM on the  $^{87}\text{Rb } 5S_{1/2} - 5P_{1/2}$  transition – but it is also known that grey molasses is effective on the  $5S_{1/2} - 5P_{3/2}$  transition [33], and future studies could compare the salient molecular physics in each manifold [35]. Further, we expect our work will be the start of explorations of the interplay of collisions and cooling in microtraps for a host of blue-detuned cooling mechanisms both for alkali atoms, as well as a variety of other atomic species and molecules.

We thank Yiheng Lin, Kai-Niklas Schymik, Ludovic Brossard, Junling Long, and Brian Lester for technical assistance, and Jose D’Incao, Paul Julienne, Ana Maria Rey, and Adam Kaufman for helpful comments and fruitful discussion. We acknowledge funding from ONR Grant No. N00014-17-1-2245, NSF Grant No. PHYS 1734006, the Cottrell Scholars program, and the David and Lucile Packard Foundation. M. O. B. acknowledges support from an NDSEG Fellowship. T.T. acknowledges funding from SNF under project number: P2EZP2\_172208.

\* These authors contributed equally

† regal@colorado.edu

- [1] W. S. Bakr, J. I. Gillen, A. Peng, S. Fölling, and M. Greiner, “A quantum gas microscope for detecting single atoms in a hubbard-regime optical lattice,” *Nature (London)* **462**, 74 (2009).
- [2] J. F. Sherson, C. Weitenberg, M. Endres, M. Cheneau, I. Bloch, and S. Kuhr, “Single-atom-resolved fluorescence imaging of an atomic Mott insulator,” *Nature (London)* **467**, 68 (2010).
- [3] L. Isenhower, E. Urban, X. L. Zhang, A. T. Gill, T. Henage, T. A. Johnson, T. G. Walker, and M. Saffman, “Demonstration of a neutral atom controlled-not quantum gate,” *Phys. Rev. Lett.* **104**, 010503 (2010).
- [4] T. Wilk, A. Gaëtan, C. Evellin, J. Wolters, Y. Miroshnychenko, P. Grangier, and A. Browaeys, “Entanglement of two individual neutral atoms using rydberg blockade,” *Phys. Rev. Lett.* **104**, 010502 (2010).
- [5] A. M. Kaufman, B. J. Lester, C. M. Reynolds, M. L. Wall, M. Foss-Feig, K. R. A. Hazzard, A. M. Rey, and C. A. Regal, “Two-particle quantum interference in tunnel-coupled optical tweezers,” *Science* **345**, 306–309 (2014).
- [6] A. M. Kaufman, B. J. Lester, M. Foss-Feig, M. L. Wall, A. M. Rey, and C. A. Regal, “Entangling two transportable neutral atoms via local spin exchange,” *Nature (London)* **527**, 208–211 (2015).
- [7] D. S. Weiss, J. Vala, A. V. Thapliyal, S. Myrgren, U. Vazirani, and K. B. Whaley, “Another way to approach zero entropy for a finite system of atoms,” *Phys. Rev. A* **70**, 040302(R) (2004).
- [8] Y. Miroshnychenko, W. Alt, I. Dotsenko, L. Förster, M. Khudaverdyan, D. Meschede, D. Schrader, and

A. Rauschenbeutel, "Quantum engineering: An atom-sorting machine," *Nature (London)* **442**, 151 (2006).

[9] M. Endres, H. Bernien, A. Keesling, H. Levine, E. R. Anschuetz, A. Krajenbrink, C. Senko, V. Vuletic, M. Greiner, and M. D. Lukin, "Atom-by-atom assembly of defect-free one-dimensional cold atom arrays," *Science* **354**, 1024–1027 (2016).

[10] D. Barredo, S. de Léséleuc, V. Lienhard, T. Lahaye, and A. Browaeys, "An atom-by-atom assembler of defect-free arbitrary two-dimensional atomic arrays," *Science* **354**, 1021–1023 (2016).

[11] H. Bernien, S. Schwartz, A. Keesling, H. Levine, A. Omran, H. Pichler, S. Choi, A. S. Zibrov, M. Endres, M. Greiner, V. Vuletić, and M. D. Lukin, "Probing many-body dynamics on a 51-atom quantum simulator," *Nature* **551**, 579–584 (2017).

[12] M. Marcuzzi, J. Minář, D. Barredo, S. de Léséleuc, H. Labuhn, T. Lahaye, A. Browaeys, E. Levi, and I. Lesanovsky, "Facilitation dynamics and localization phenomena in rydberg lattice gases with position disorder," *Phys. Rev. Lett.* **118**, 063606 (2017).

[13] W. Lee, H. Kim, and J. Ahn, "Defect-free atomic array formation using the Hungarian matching algorithm," *Phys. Rev. A* **95**, 053424 (2017).

[14] D. Barredo, V. Lienhard, S. de Léséleuc, T. Lahaye, and A. Browaeys, "Synthetic three-dimensional atomic structures assembled atom by atom," *Nature* **561**, 79–82 (2018).

[15] A. Kumar, T.-Y. Wu, F. Giraldo, and D. S. Weiss, "Sorting ultracold atoms in a three-dimensional optical lattice in a realization of Maxwell's demon," *Nature* **561**, 83–87 (2018).

[16] A. T. Grier, I. Ferrier-Barbut, B. S. Rem, M. Delehaye, L. Khaykovich, F. Chevy, and C. Salomon, "Λ-enhanced sub-doppler cooling of lithium atoms in  $D_1$  gray molasses," *Phys. Rev. A* **87**, 063411 (2013).

[17] D. Rio Fernandes, F. Sievers, N. Kretzschmar, S. Wu, C. Salomon, and F. Chevy, "Sub-doppler laser cooling of fermionic 40 k atoms in three-dimensional gray optical molasses," *Europhys. Lett.* **100**, 63001 (2012).

[18] N. Schlosser, G. Reymond, I. Protsenko, and P. Grangier, "Sub-poissonian loading of single atoms in a microscopic dipole trap," *Nature (London)* **411**, 1024 (2001).

[19] T. Grünzweig, A. Hilliard, M. McGovern, and M. F. Andersen, "Near-deterministic preparation of a single atom in an optical microtrap," *Nat. Phys.* **6**, 951–954 (2010).

[20] N. Schlosser, G. Reymond, and P. Grangier, "Collisional blockade in microscopic optical dipole traps," *Phys. Rev. Lett.* **89**, 023005 (2002).

[21] A. V. Carpentier, Y. H. Fung, P. Sompet, A. J. Hilliard, T. G. Walker, and M. F. Andersen, "Preparation of a single atom in an optical microtrap," *Laser Phys. Lett.* **10**, 125501 (2013).

[22] B. J. Lester, N. Luick, A. M. Kaufman, C. M. Reynolds, and Cindy A. Regal, "Rapid production of uniformly filled arrays of neutral atoms," *Phys. Rev. Lett.* **115**, 073003 (2015).

[23] Y. H. Fung and M. F. Andersen, "Efficient collisional blockade loading of a single atom into a tight microtrap," *New J. Phys.* **17**, 073011 (2015).

[24] A. Aspect, E. Arimondo, R. Kaiser, N. Vansteenkiste, and C. Cohen-Tannoudji, "Laser cooling below the one-photon recoil energy by velocity-selective coherent population trapping," *Phys. Rev. Lett.* **61**, 826–829 (1988).

[25] M. S. Shahriar, P. R. Hemmer, M. G. Prentiss, P. Marte, J. Mervis, D. P. Katz, N. P. Bigelow, and T. Cai, "Continuous polarization-gradient precooling-assisted velocity-selective coherent population trapping," *Phys. Rev. A* **48**, R4035–R4038 (1993).

[26] G. Grynberg and J.-Y. Courtois, "Proposal for a magneto-optical lattice for trapping atoms in nearly-dark states," *Europhys. Lett.* **27**, 41 (1994).

[27] T. Esslinger, F. Sander, A. Hemmerich, T. W. Hänsch, H. Ritsch, and M. Weidemüller, "Purely optical dark lattice," *Opt. Lett.* **21**, 991–993 (1996).

[28] D. J. McCarron, E. B. Norrgard, M. H. Steinecker, and D. DeMille, "Improved magneto-optical trapping of a diatomic molecule," *New J. Phys.* **17**, 035014 (2015).

[29] J. A. Devlin and M. R. Tarbutt, "Three-dimensional doppler, polarization-gradient, and magneto-optical forces for atoms and molecules with dark states," *New J. Phys.* **18**, 123017 (2016).

[30] L. W. Cheuk, L. Anderegg, B. L. Augenbraun, Y. Bao, S. Burchesky, W. Ketterle, and J. M. Doyle, "Λ-enhanced imaging of molecules in an optical trap," *Phys. Rev. Lett.* **121**, 083201 (2018).

[31] J. Lim, J. R. Almond, M. A. Trigatzis, J. A. Devlin, N. J. Fitch, B. E. Sauer, M. R. Tarbutt, and E. A. Hinds, "Laser cooled YbF molecules for measuring the electron's electric dipole moment," *Phys. Rev. Lett.* **120**, 123201 (2018).

[32] L. Anderegg, B. L. Augenbraun, Y. Bao, S. Burchesky, L. W. Cheuk, W. Ketterle, and J. M. Doyle, "Laser cooling of optically trapped molecules," *Nat. Phys.* **14**, 890–893 (2018).

[33] S. Rosi, A. Burchianti, S. Conclave, D. S. Naik, G. Roati, C. Fort, and F. Minardi, "Λ-enhanced grey molasses on the  $D_2$  transition of rubidium-87 atoms," *Sci. Rep.* **8**, 1301 (2018).

[34] A. M. Kaufman, *Laser-cooling atoms to indistinguishability: Atomic Hong-Ou-Mandel interference and entanglement through spin exchange*, Ph.D. thesis, University of Colorado at Boulder (2015).

[35] J. Weiner, V. S. Bagnato, S. Zilio, and P. S. Julienne, "Experiments and theory in cold and ultracold collisions," *Rev. Mod. Phys.* **71**, 1–85 (1999).

[36] F. L. Kien, P. Schneeweiss, and A. Rauschenbeutel, "Dynamical polarizability of atoms in arbitrary light fields: general theory and application to cesium," *Eur. Phys. J. D* **67**, 92 (2013).

[37] L. D. Brown, T. T. Cai, and A. DasGupta, "Interval estimation for a binomial proportion," *Stat. Sci.* **16**, 101–117 (2001).

## APPENDIX

### Optical Tweezers

We generate an array of optical-tweezer traps spaced by 2  $\mu\text{m}$  in the  $xy$ -plane by passing a single 850 nm laser beam through two orthogonal longitudinal-wave  $\text{TeO}_2$  acousto-optical modulators (AOMs) with center frequencies (bandwidths) of 180 MHz (90 MHz). Each modulator is driven with a sum of radio-frequency (RF) tones with frequency (amplitude) that can be individ-

ually and dynamically adjusted to control the position (intensity) of different tweezer-rows and columns. The relative phases of the tones are set to minimize intermodulation in the RF setup. The array of deflections created by the AOMs is then imaged by a 0.6-NA-objective lens into a glass cell. This creates a trap with a  $0.68\text{ }\mu\text{m}$  waist for a single tweezer, and traps with an average waist of  $0.75\text{ }\mu\text{m}$  for a  $10 \times 10$  array. The standard deviation of the trap depths was minimized to 8% by optimizing the RF amplitudes. Trap depths are calibrated by measuring light-shifts of in-trap atomic transitions as a function of trap power [36]. The lifetime of atoms in the traps is limited to 5 s by the background pressure.

### Laser Cooling and Loading

In all experiments, three beam paths are used to address the atoms. Two (diagonal) paths are along the diagonals of the  $xy$ -plane, and a third (acute) path in the  $xz$ -plane is at an angle of  $55^\circ$  from the  $z$ -axis to avoid the objective [34]. All lasers along these paths are retro-reflected and in a  $\sigma^+\sigma^-$  polarization configuration.

Our magneto-optical trap (MOT) is spatially overlapped with the trap array and cools atoms for 500 ms to a temperature of  $\sim 100\text{ }\mu\text{K}$ , measured by imaging its ballistic expansion. The cooling (repump) laser is red-detuned from the  $D_2\text{ }|F=2\rangle \rightarrow |F''=3\rangle$  ( $|F=1\rangle \rightarrow |F''=2\rangle$ ) transition, and applied on all three beam paths (on only the diagonal paths). In the case of the 20-ms-long RPGC stage we cool the atoms to  $\sim 10\text{ }\mu\text{K}$ . For this, we detune the cooling (repump) laser by  $\Delta_{\text{RPGC}}$  (20 MHz), set the intensities at  $1.3\text{ }I_{\text{sat}}$  ( $0.1\text{ }I_{\text{sat}}$ ) on the diagonal paths and  $4.5\text{ }I_{\text{sat}}$  ( $0\text{ }I_{\text{sat}}$ ) on the acute path, and zero the magnetic fields.

In the case of the 200-ms-long  $\Lambda$ -enhanced gray molasses (AGM) stage, we apply a cooling laser that is detuned by  $\Delta_{\text{AGM}}$  from the  $D_1\text{ }|F=2\rangle \rightarrow |F'=2\rangle$  transi-

sition at  $2.5\text{ }I_{\text{sat}}$  ( $0.4\text{ }I_{\text{sat}}$ ) on the acute (diagonal) paths. We create the coherent repump beam from the cooling laser on the acute path using an electro-optic modulator. The repump beam is detuned by  $\Delta_{\text{AGM}} + 0.14\text{ MHz}$  from the  $D_1\text{ }|F=1\rangle \rightarrow |F'=2\rangle$  transition and at  $1.5\text{ }I_{\text{sat}}$ . Note that the optimal AGM free-space temperature of  $50\text{ }\mu\text{K}$  is reached for  $\Delta_{\text{AGM}} \approx 15\text{ MHz}$  and is likely limited by the beam path geometry and repump light configuration.

### Imaging, Data, and Statistics

Regardless of the loading configuration, we image the atoms using another RPGC stage with the cooling beam ( $\Delta_{\text{RPGC}} = 19\text{ MHz}$  at  $3\text{ }I_{\text{sat}}$ ) only on the acute path. We alternate the tweezer-light with the imaging light at 2 MHz to scatter light when atoms are experiencing no light shifts. This configuration is maintained for 20 ms during which we collect scattered photons on an EMCCD camera, superbinned to  $4 \times 4$  pixels to reduce readout noise.

At every atom location individually, to determine a count threshold that indicates the presence of an atom in the trap, we create a histogram of all counts during an experiment and fit it with a sum of two Gaussians. The threshold with maximal fidelity  $\mathcal{F}$  is found, where  $\mathcal{F} = 1 - (E_{fp} + E_{fn})$ , with  $E_{fp}$  ( $E_{fn}$ ) being the expected rate of false positives (false negatives) from the fits. This converts a sequence of counts to a sequence of Booleans which is averaged to determine the loading probability. All errors reported indicate  $1\sigma$  equal-tailed Jeffrey's prior confidence intervals [37]. The loading efficiencies reported in the main text for RPGC (64(1)%), AGM (89(1)%), and  $10 \times 10$ -AGM (80.49(6)% were obtained by analyzing 2000, 1000, and 1000-per-atom repetitions with threshold fidelities 0.987, 0.998, and 0.993 respectively.